

# Chapter Number 25

## Dynamical Enhancement Technique for Geophysical Analysis of Remote Sensing Imagery

Iván E. Villalón-Turrubiates

*University of Guadalajara Campus Los Valles*

*Guadalajara–Ameca Highway Km. 45.5, 46600 Ameca Jalisco, Mexico*

*Telephone (+52 37) 5758-0148 ext. 7267, E-Mail: villalon@ieee.org*

### 1. Introduction

Considerable progress has been made generally in the application of remote sensing techniques to both research and operational problems for urban planning and natural resource management. Modern applied theory of image processing is now a mature and well developed research field, presented and detailed in many works.

Although the existing theory offers a manifold of statistical techniques to tackle with the particular environmental monitoring problems, in many applications areas there still remain some crucial theoretical and data processing problems. One of them is particularly related to the extraction and dynamical analysis of physical characteristics (e.g., water, land cover, vegetation, soil, humid content, and dry content) for implementation in natural resources management (modeling and planning).

The extraction of environmental physical characteristics from a particular geographical region through remote sensing data processing allows the generation of electronic signature maps, which are the basis to create a high-resolution collection atlas processed in time for a particular geographical zone. This can be achieved using a systematical tool for supervised segmentation and classification of the environmental remote sensing signatures that employs multispectral remote sensing imagery based on pixel statistics for the class description. Moreover, the analysis of a dynamical model of environmental characteristics extracted from a geographic region generates useful information for natural resource management; using the signatures map extracted from the remote sensing imagery for a particular geographic zone in discrete time the evolution study of the environmental characteristics is performed to obtain the dynamical model of the physical variables. This provides a background for understanding the future trends of the multispectral image. This chapter explores the implementation possibilities of the multispectral image classification technique with the dynamic analysis for natural resources management applications.

#### 1.1 Remote Sensing

The goal of science is to discover universal truths that are the same yesterday, today and tomorrow. Hopefully, the knowledge obtained can be used to protect the environment and improve human quality of life. To identify these universal truths, scientists observe and make measurements about (a) the physical world (e.g., the atmosphere, water, soil, rock), (b)

its living inhabitants (e.g., *Homo sapiens*, flora, fauna), and (c) the process at work (e.g., mass wasting, deforestation, urban sprawl).

Scientists formulate hypotheses and then attempt to accept or reject them in a systematic, unbiased fashion. The data necessary to accept or reject a hypothesis may be collected directly in the field, often referred to as *in situ* or *in place* data collection. This can be a time-consuming, expensive, and inaccurate process. Therefore, considerable research during the past century has gone into the development of aerial platforms (e.g., suborbital aircraft, satellites, unmanned aerial vehicles) and sensors (e.g., cameras, detectors) that can collect information some remote distance from the subject (e.g., from 10,000 meters above ground level). This process is called remote sensing (RS) of the environment (Jensen, 2005).

The remote sensor data can be stored in an analog format (e.g., a hardcopy 9×9 in. vertical aerial photograph) or in a digital format (e.g., remote sensing imagery consisting up to seven registered matrices of brightness values). The analog and digital remote sensing data can be analyzed using analog (visual) and/or digital image processing techniques.

A science is defined as the broad field of human knowledge concerned with facts held together by principles (rules). Scientists discover and test facts and principles by the scientific method, and orderly system of solving problems. Scientists generally feel that any subject that humans can study by using the scientific method and other special rules of thinking may be called a science. The science includes (a) mathematics and logic, (b) the physical sciences, such as physics and chemistry, (c) the biological sciences, such as botany and zoology, and (d) the social sciences, such as geography, sociology, anthropology, etc. Interestingly, some persons do not consider mathematics and logic to be sciences. But the fields of knowledge associated with mathematics and logic are such valuable tools for science that cannot be ignored.

Remote sensing is a tool or technique similar to mathematics. Using sensors to measure the amount of electromagnetic radiation (EMR) existing an object or geographic area from a distance and the extracting valuable information from the data using mathematically and statistically based algorithms is a scientific activity (Jensen, 2005). It functions in harmony with other spatial data collections techniques or tools of the mapping sciences, including geographic information systems (GIS) (Fussell et al., 1986).

The process of visual photo or image interpretation brings to bear not only scientific knowledge but all of the background that a person has obtained in his lifetime. Such learning cannot be measured, programmed or completely understood. The synergism of combining scientific knowledge with real-world analyst experience allows the interpreter to develop heuristic rules of thumb to extract information from the imagery. Some image analysts are superior to other image analysts because they (a) understand the scientific principles better, (b) are more widely traveled and have seen many landscape objects and geographic areas, and/or (c) have the ability to synthesize principles and real-world knowledge to reach logical and correct conclusions. The remote sensing image interpretation is both an art and a science (Jensen, 2005).

Sensors can be used to obtain very specific information about an object (e.g., the diameter of a cottonwood tree's crowns) or the geographic extent of a phenomenon (e.g., the polygonal boundary of a cottonwood stand). The EMR reflected, emitted, or back-scattered from an object or geographical area is used as a surrogate for the actual property under investigation. The electromagnetic energy measurements must be calibrated and turned into information using visual and/or digital image processing techniques.

Urban planners (e.g., land use, transportation, utility) and natural resource management (e.g., wetland, forest, grassland, rangeland) recognize that spatially distributed information

is essential for ecological modeling and planning. Unfortunately, it is very difficult to obtain such information using in situ measurements. Therefore, public agencies and scientists have expanded significant resources in developing methods to obtain the required information using remote sensing science (Shkvarko & Villalon, 2007).

## 1.2 Image Interpretation

The classical process of classification consists of two stages (Smith, 2000). The first is the recognition of categories of real-world objects (segmentation). In the context of multispectral remote sensing (MRS) of the land surface these categories could include, for example, woodlands, water bodies, grassland and other land cover types, depending on the geographical scale and nature of the study. The second stage is the labeling of the entities (classification) that are to be classified.

In digital image classification these labels are numerical, so that a pixel that is recognized as belonging to the class 'water' may be given the label '1', 'woodland' may be labeled '2', and so on. The process of image classification requires the user to perform the following steps: (a) determine a-priori the number and nature of the categories in terms of which environmental remote sensing signatures (RSS) are to be described, and (b) assign numerical labels to the pixels on the basis of their RSS properties using a decision-making procedure, usually termed a classification rule or a decision rule.

Clustering is a kind of exploratory procedure, the aim of which is to determine the number (but not initially the identity) of distinct RSS present in the area covered by the image, and to allocate pixels to these categories in terms of the nature of the RSS types is a separate stage that follows the clustering procedure. Several clusters may correspond to a single RSS type (Smith, 2000).

These two approaches to pixel labeling are known in the RS literature as supervised and unsupervised classification procedures, respectively (Smith, 2000). They can be used to segment an image into regions with similar attributes. In the simplest case, a pixel is characterized by a vector whose elements are its grey levels in each spectral band. This vector represents the spectral properties of that pixel.

In a supervised classification, the identity and location of some of the RSS types (e.g., urban, agriculture or wetland) are known a priori through a combination of field work, interpretation of aerial photography, map analysis or personal experience. The analyst attempts to locate specific sites in the MRS data that represents homogeneous examples of these known RSS types. These areas are commonly referred to as training sites because the spectral characteristics of these known areas are used to train the classification algorithm for eventual RSS mapping of the remainder of the image. Multivariate statistical parameters (means, standard deviations, covariance matrices, correlation matrices, etc.) are calculated for each training site. Every pixel both within and outside the training sites is then evaluated and assigned to the class of which it has the highest likelihood of being a member (Jensen, 2005).

In an unsupervised classification, the identities of RSS types to be specified as classes within a scene are not generally known a priori because ground reference information is lacking or surface features within the scene are not well defined. The computer is required to group pixels with similar spectral characteristics into unique clusters according to some statistical determined criteria. The analyst then re-labels and combines the RSS spectral clusters into formation classes (Jensen, 2005).

The term dynamic refers to phenomena that produce time-changing pattern, the characteristics of the pattern at one time being interrelated with those at other times. The term is nearly

synonymous with time-evolution or pattern of change (Luenberger, 1979). Nearly all observed phenomena in our daily lives or in scientific investigation have important dynamic aspects. Scientific examples may arise in (a) a physical system, such as a signal traveling through the space, a home heating system, or in the mining of a mineral deposit, (b) a social system, such as the movement within an organization hierarchy, the evolution of a tribal class system, or the behavior of an economic structure, and (c) a life system, such as that of genetic transference, ecological decay, or population growth.

Many dynamic systems can be understood and analyzed intuitively, without resort to mathematics and without development of a general theory of dynamics. However, in order to approach unfamiliar complex situations efficiently, it is necessary to proceed systematically. Mathematics can provide the required economy of language and conceptual framework.

The term dynamics takes a dual meaning. It is a term for the time-evolutionary phenomena in the world about us, and a term for that part of mathematical science that is used for the representation and analysis of such phenomena (Luenberger, 1979). Dynamic systems are represented mathematically in terms of either differential or difference equations. These equations provide the structure for representing time linkages among variables. The use of either differential or difference equations to represent dynamic behavior corresponds, respectively, to whether the behavior is viewed as occurring in continuous or discrete time.

Continuous time corresponds to our usual conception, where time is regarded as a continuous variable and is often viewed as flowing smoothly past us (Luenberger, 1979). In mathematical terms, continuous time of this sort is quantified in terms of the continuum of real numbers.

Discrete time consists of an ordered sequence of points rather than a continuum. In terms of applications, it is convenient to introduce this kind of time when events and consequences either occurring are accounted for only at discrete time periods, such as daily, monthly, or yearly. Accordingly dynamic behavior viewed in discrete time is usually described by equations relating the value of a variable at one time to the values at adjacent times. Such equations are called difference equations.

## 2. Multispectral Image Classification

Multispectral imaging is a technology originally developed for space-based imaging. The multispectral images are the main type of images acquired by MRS radiometers. Usually, MRS systems have from 3 to 7 radiometers; each one acquires one digital image (also called scene) in a small band of visible spectra, ranging 450 nm to 690 nm, called red-green-blue (RGB) regions (Villalon, 2008).

For different purposes, combinations of spectral bands can be used. They are usually represented with red (R), green (G) and blue (B) channels. This is referred to as True-Color RS imagery (Villalon, 2008). The wavelengths for the spectral bands are as follows, where the values are approximated, exact values depends on the particular RS instruments (Mather, 2004): (a) blue: 450-520 nm, (b) green: 520-600 nm, and (c) red: 600-690 nm.

### 2.1 Weighted Order Statistics method

The WOS method is a generalization of the median filter (Perry et al., 2002), and is characterized by a weight vector and a threshold value. The order statistics (OS) filtering methodology (Yli-Harja et al., 1991) shifts a  $n \times n$  window  $\mathbf{W}$  (with cardinality  $n \times n$ , i.e.,  $|\mathbf{W}| = n \times n$ )

over an input RS image frame and, at each position of the frame, takes the  $n \times n$  inputs ( $w_{11}, w_{12}, \dots, w_{ij}, \dots, w_{nn}$ ) under  $\mathbf{W}_{ij}$  and then outputs the  $r$ -th element of the sorted input.

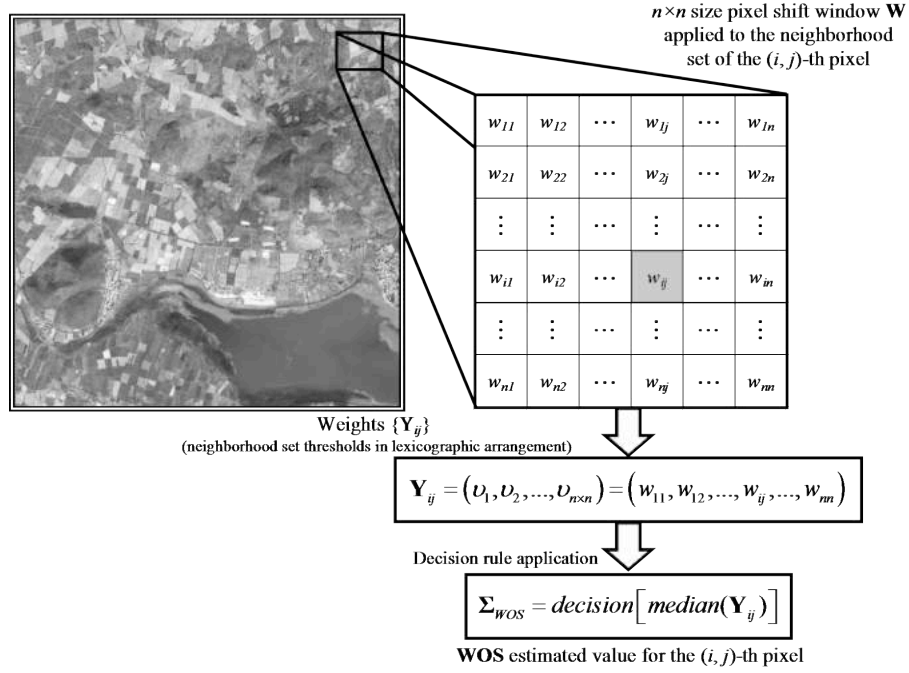


Fig. 1. Weighted order statistics filtering method

The WOS method is a generalization of the OS filter that is characterized by a weight vector  $\mathbf{Y}_{ij} = (v_1, v_2, \dots, v_{n \times n})$  of  $n \times n$  positive weight thresholds  $w$ ,  $0 \leq w \leq 255$  (gray-level threshold). To compute the output, each input  $w$  is duplicated to the number of corresponding weight  $v$ , then they are sorted and the  $w$ -th order element is chosen as the output, expressed as

$$\mathbf{WOS}_{ij} = \text{median}(\mathbf{Y}_{ij}), \quad (1)$$

where  $\mathbf{WOS}_{ij}$  is the weighted order of the  $(i, j)$ -th pixel of the image. The decision rule for classification based on the WOS filter determines that, based on the a priori information for class segmentation (number of RSS to be classified and their respective thresholds), the WOS value for each image pixel is compared with the a priori thresholds (gray-level) and classified according to the most proximal value. Fig. 1 shows the process structure of the WOS filter.

## 2.2 Minimum Distance to Means method

The MDM decision rule is computationally simple and can result in classification accuracy comparable to other more computationally intensive algorithms (Jensen, 2005). It is characterized by the mean values of the RSS classes and the Euclidean distances based on the Py-

thagorean Theorem. An important aspect of this method is that it is applied to the MRS imagery. The a priori information for class segmentation (number of RSS to be classified and their respective mean values) conform the means matrix  $\mathbf{E}$  ( $c \times b$  size) that contains the mean values  $\mu_{cb}$ : ( $0 \leq \mu_{cb} \leq 255$ , gray-level) of the RSS classes for every MRS band. Here,  $c$  is the number of RSS classes to be classified, and  $b$  is the number of spectral bands.

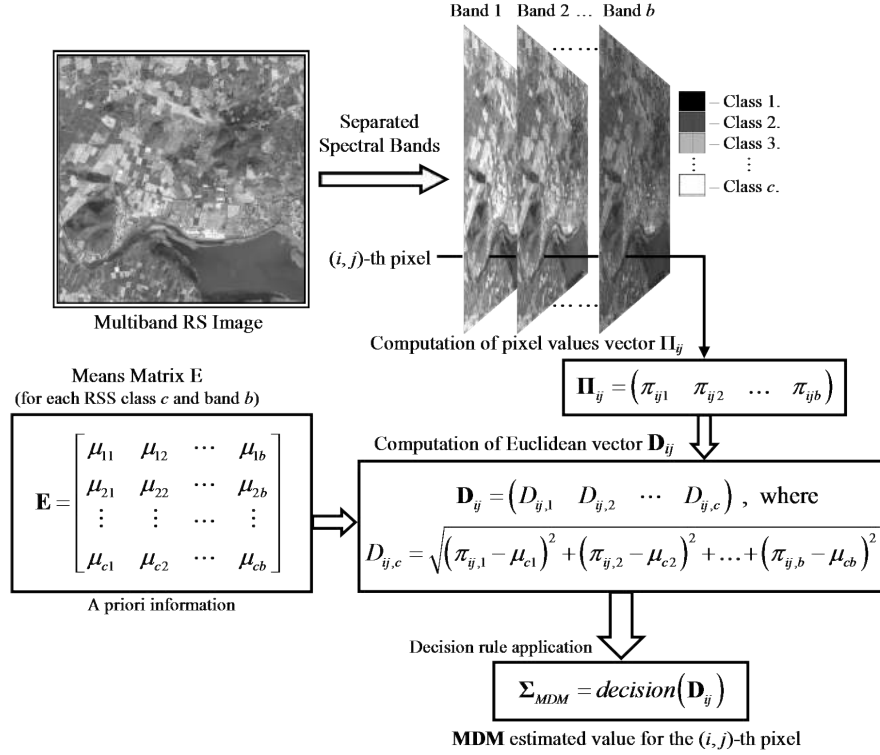


Fig. 2. Minimum distance to means method

The input is defined by the vector  $\Pi_{ij}$ , which contains the  $(i, j)$ -th image pixel values  $\pi_{ijb}$  employed for every spectral band. To compute the output of the classifier, the distance between each input  $\Pi_{ij}$  and the means matrix  $\mathbf{E}$  is calculated using the Euclidean distance based on the Pythagorean Theorem. This is expressed as

$$\mathbf{D}_{ij,c} = \sqrt{(\pi_{ij,1} - \mu_{c1})^2 + (\pi_{ij,2} - \mu_{c2})^2 + \dots + (\pi_{ij,b} - \mu_{cb})^2}, \quad (2)$$

where  $\mathbf{D}_{ij,c}$  is a vector ordered by multi-index  $(ij,c)$  of  $c \times 1$  size that contains the distances between the  $(i, j)$ -th image pixel value and the  $c$ -class value for each band  $b$ .

The decision rule for classification based on the MDM filter determines that, based on the a priori information for class segmentation (number of RSS to classify and their respective mean values), each image pixel generates an ordered distance vector  $\mathbf{D}_{ij}$ , and therefore, the

pixel is classified according to the minimum value on the vector. Fig. 2 shows the processing structure of the MDM classifier.

### 2.3 Weighted Pixel Statistics method

The Weighted Pixel Statistics (WPS) classificatory rule is computationally simple and can result in classification accuracy comparable to other more computationally intensive algorithms (WOS and MDM methods). It is characterized by the mean and variance values of the RSS signatures (classes) and the Euclidean distances based on the Pythagorean Theorem. An important aspect of this method is that it is applied to the MRS imagery.

The training data for class segmentation requires the number of RSS to be classified ( $c$ ); the means matrix  $\mathbf{M}$  ( $c \times c$  size) that contains the mean values  $\mu_{cc}$ : ( $0 \leq \mu_{cc} \leq 255$ , gray-level) of the RSS classes for each RGB bands; and the variances matrix  $\mathbf{V}$  ( $c \times c$  size) that contains the variances of the RSS classes for each RGB bands. The matrix  $\mathbf{M}$  and  $\mathbf{V}$  represents the weights of the classification process. Next, the image is separated in the spectral bands (R, G and B) and each  $(i, j)$ -th pixel is statistically analyzed calculating the means and variances from a neighborhood set of  $5 \times 5$  pixels for each RGB band, respectively. To compute the output of the classifier, the distances between the pixel statistics and the training data is calculated using Euclidean distances based on the Pythagorean Theorem for means and variances, respectively. The decision rule used by the WPS method is based on the minimum distances gained between the weighted training data and the pixel statistics.

The WPS techniques provide a high level of RSS segmentation and classification. Figure 3 shows the detailed processing structure of the WPS classifier.

## 3. Dynamic Model of Remote Sensing Signatures

This is a new innovative paradigm for mathematical analysis of the space-time dynamic evolution of the particular environmental RSS extracted from MRS images in evolution time. This is performed via the Geophysical Dynamic Laboratory (GDL) method, which unifies the RSS mapping scheme with its dynamic analysis to provide the high-resolution mapping of the RSS in evolution time. If the attributes of interest of a system are changing with time, then it is referred to a dynamic system. A RSS process is the evolution over time of such a dynamic system (Grewal & Andrews, 2001).

### 3.1 Mathematical model of RSS in continuous time

The model of a RSS of interest treated as a linear dynamic system (LDS) is presented in its state variables (Falkovich et al., 1989) described over the continuous evolution time (CET) domain ( $\tau \in \mathfrak{T}$ ) and the discrete evolution time (DET) domain ( $\kappa \in \mathfrak{X}$ ). A LDS is represented in CET and DET as shown in Fig. 4(a) and 4(b), respectively, where  $\Sigma(\tau)$  and  $\{\Sigma(\kappa)\}$  are the inputs to the linear system,  $\Lambda(\tau)$  and  $\{\Lambda(\kappa)\}$  are the outputs of the linear system, respectively.

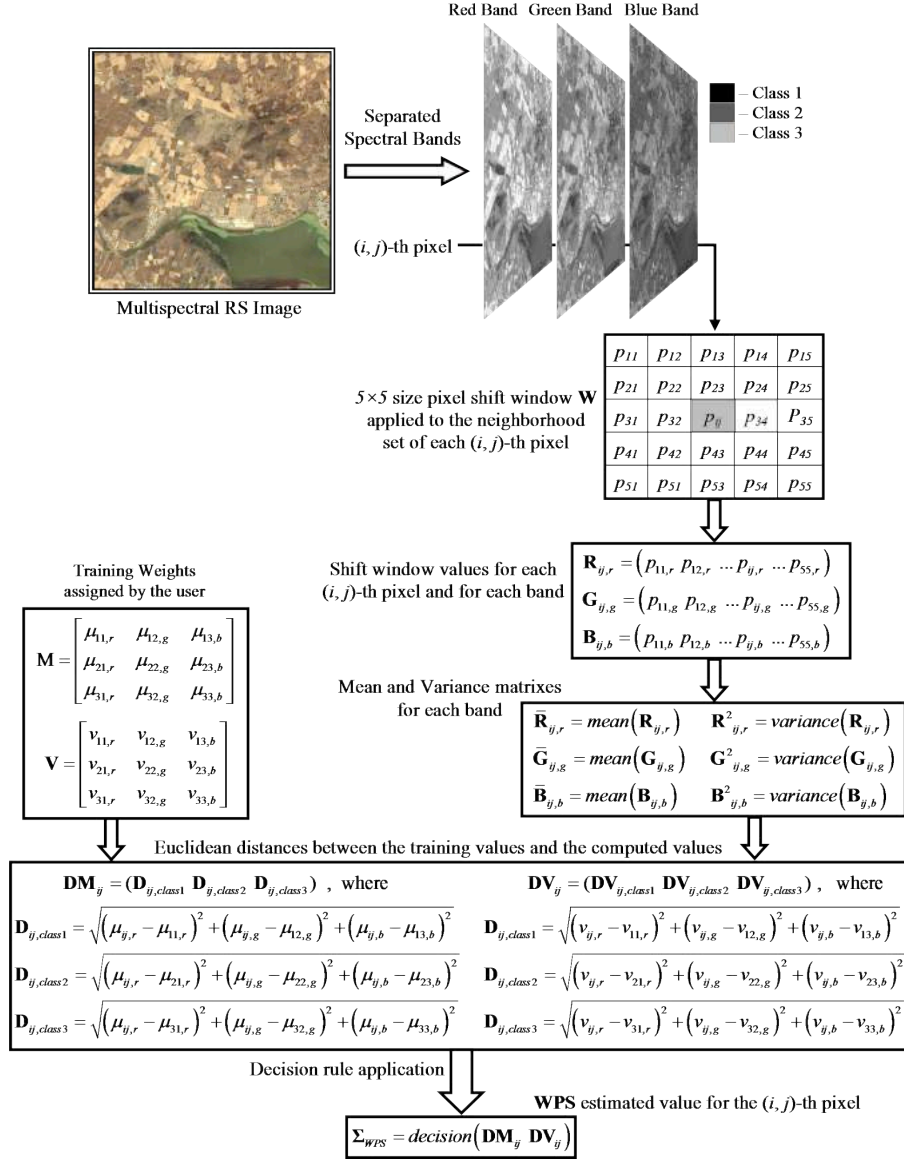


Fig. 3. Computational structure of the WPS method

The model of the equation of observation (EO) in CET is represented (Falkovich et al., 1989) as  $\Sigma(\tau) = S(\Lambda(\tau)) + \nu(\tau)$ , where  $\nu(\tau)$  is the white observation Gaussian noise and  $\tau \in \mathcal{T}$ , starting at  $\tau_0$  (initial moment of continuous evolution time), and the linear amplitude-modulated



(Falkovich et al., 1989) model is  $S(\Lambda(\tau)) = \Lambda(\tau)S_0(\tau)$ , where  $S_0(\tau)$  represents the deterministic “carrier” RS image frame of a given model, and  $\Lambda(\tau)$  is the unknown stochastic information process to be estimated via processing of the MRS image observation data frame  $\Sigma(\tau)$ .

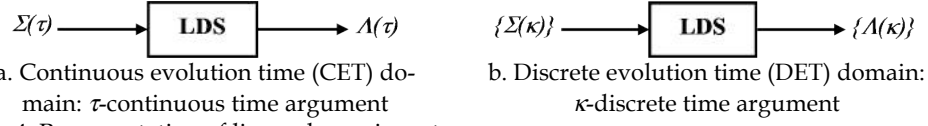


Fig. 4. Representation of linear dynamic systems

It is assumed that  $\Lambda(\tau)$  satisfies the dynamical model specified by the following  $N$ -th order linear differential equation (Villalon & Shkvarko, 2008)

$$\frac{d^N \Lambda(\tau)}{d\tau^N} + \alpha_{N-1} \frac{d^{N-1} \Lambda(\tau)}{d\tau^{N-1}} + \dots + \alpha_0 \Lambda(\tau) = \beta_{N-1} \frac{d^{N-1} \xi(\tau)}{d\tau^{N-1}} + \dots + \beta_0 \xi(\tau). \quad (3)$$

where  $\alpha$  and  $\beta$  are the constant coefficients of the dynamical system model for evolution of the RSS  $\Lambda(\tau)$ . This stochastic model can be redefined as follows: the differential equation (3) may be transformed into a system of linear differential equations of the first order via performing the following replacement of variables

$$\left\{ \begin{array}{l} z_1(\tau) = \Lambda(\tau), \\ z_2(\tau) = \frac{dz_1(\tau)}{d\tau} + \alpha_{N-1} z_1(\tau) - \beta_{N-1} \xi(\tau), \\ \dots \\ z_N(\tau) = \frac{dz_{N-1}(\tau)}{d\tau} + \alpha_1 z_1(\tau) - \beta_1 \xi(\tau), \\ \frac{dz_N(\tau)}{d\tau} = -\alpha_0 z_1(\tau) + \beta_0 \xi(\tau) \end{array} \right. \quad (4)$$

where

$$\mathbf{z}(\tau) = (z_1(\tau) \ z_2(\tau) \ \dots \ z_N(\tau))^T. \quad (5)$$

Based on the replacement of variables specified by (4), the dynamic differential equation model (3) can be now represented in a canonical vector-matrix form as follows

$$\frac{d\mathbf{z}(\tau)}{d\tau} = \mathbf{F}\mathbf{z}(\tau) + \mathbf{G}\xi(\tau), \quad \Lambda(\tau) = \mathbf{C}\mathbf{z}(\tau). \quad (6)$$

where

$$\mathbf{F} = \begin{bmatrix} -\alpha_{N-1} & 1 & 0 & \dots & 0 \\ -\alpha_{N-2} & 0 & 1 & \dots & 0 \\ \dots & \dots & \dots & \dots & \dots \\ -\alpha_1 & 0 & 0 & \dots & 1 \\ -\alpha_0 & 0 & 0 & \dots & 0 \end{bmatrix}, \quad \mathbf{G} = \begin{bmatrix} \beta_{N-1} \\ \beta_{N-2} \\ \dots \\ \beta_0 \end{bmatrix}, \quad \mathbf{C} = [1 \mid 0 \dots 0]. \quad (7)$$

The representation in the form of (6) is referred to as a canonical equation of linear dynamic system in state variables in continuous time. Here,  $\mathbf{z}(\tau)$  is the state vector, the vector  $\mathbf{C}$  defines a linear operator that introduces the relation between the RSS map in continuous time and the state vector  $\mathbf{z}(\tau)$ ,  $\mathbf{F}$  is a transition matrix,  $\mathbf{G}$  is a transition vector, and  $\xi(\tau)$  represents the white model generation noise vector characterized by the statistics,  $\langle \xi(\tau) \rangle = \mathbf{0}$  and  $\langle \xi(\tau) \xi^T(\tau') \rangle = \mathbf{P}_\xi(\tau) \sigma(\tau - \tau')$ , respectively. Here,  $\mathbf{P}_\xi(\tau)$  is referred to as state model disperse matrix that characterizes the dynamics of the state variances developed in continuous time  $\tau$  ( $\tau_0 \rightarrow \tau$ ) starting from the initial instant  $\tau_0$ . The dynamic model equation in the continuous time states the relation between the RSS map  $\Sigma(\tau)$  extracted from the MRS scene, thus the desired dynamical RSS map  $\Lambda(\tau)$  can be represented as follows (Villalon & Shkvarko, 2008)

$$\Sigma(\tau) = \mathbf{S}_0(\tau) \mathbf{C}(\tau) \mathbf{z}(\tau) + \mathbf{v}(\tau) = \mathbf{H}(\tau) \mathbf{z}(\tau) + \mathbf{v}(\tau), \quad \text{where } \mathbf{H}(\tau) = \mathbf{S}_0(\tau) \mathbf{C}(\tau). \quad (8)$$

The stochastic differential model of equations (6) and (8) allows applying the theory of dynamical filtration to reconstruct the desired RSS map in continuous time incorporating the a priori model of dynamical information about the RSS. The aim of the dynamic filtration is to find an optimal estimate of the desired RSS,  $\hat{\Lambda}(\tau) = \mathbf{C} \hat{\mathbf{z}}(\tau)$ , developed in continuous time  $\tau$  ( $\tau_0 \rightarrow \tau$ ) via processing the RSS maps  $\Sigma(\tau)$  extracted from the MRS scenes taking into considerations the a priori dynamic model of the desired RSS map specified through the state equation (6). The optimal dynamic filter when applied to the RSS maps  $\Sigma(\tau)$  specified by the dynamic image model (8) must provide the optimal estimation of the desired RSS map  $\hat{\Lambda}(\tau) = \mathbf{C} \hat{\mathbf{z}}(\tau)$ , in which the state vector estimate  $\mathbf{z}(\tau)$  satisfies the a priori dynamic behavior modeled by the stochastic dynamic state equation (6).

### 3.2 Mathematical model of RSS in discrete time

The canonical discrete-time solution to equation (6) in state variables for discrete time  $\kappa$  is expressed as follows (Falkovich et al., 1989)

$$\mathbf{z}(\kappa+1) = \Phi(\kappa) \mathbf{z}(\kappa) + \Gamma(\kappa) \xi(\kappa), \quad \Lambda(\kappa) = \mathbf{C}(\kappa) \mathbf{z}(\kappa), \quad (9)$$

where  $\Phi(\kappa) = \mathbf{F}(\tau_\kappa)\Delta\tau + \mathbf{I}$ ;  $\Gamma(\kappa) = \mathbf{G}(\tau_\kappa)\Delta\tau$ , and  $\Delta\tau$  represents the continuous time sampling interval for dynamical modeling of the RSS map in discrete time. The statistical characteristics of the a priori information are as follows

1. Generating model noise  $\{\xi(\kappa)\}$ :

$$\langle \xi(\kappa) \rangle = \mathbf{0} ; \quad \langle \xi(\kappa)\xi^T(\kappa') \rangle = \mathbf{P}_\xi(\kappa, \kappa') . \quad (10)$$

2. Observation (RSS map) noise  $\{\mathbf{v}(\kappa)\}$ :

$$\langle \mathbf{v}(\kappa) \rangle = \mathbf{0} ; \quad \langle \mathbf{v}(\kappa)\mathbf{v}^T(\kappa') \rangle = \mathbf{P}_v(\kappa, \kappa') . \quad (11)$$

3. State vector  $\{\mathbf{z}(\kappa)\}$

$$\langle \mathbf{z}(0) \rangle = \mathbf{m}_z(0) ; \quad \langle \mathbf{z}(0)\mathbf{z}^T(0) \rangle = \mathbf{P}_z(0) . \quad (12)$$

where 0 argument implies the initial state for initial time instant ( $\kappa = 0$ ). The disperse matrix  $\mathbf{P}_z(0)$  satisfies the following disperse dynamic equation (Villalon & Shkvarko, 2008)

$$\mathbf{P}_z(\kappa+1) = \langle \mathbf{z}(\kappa+1)\mathbf{z}^T(\kappa+1) \rangle = \Phi(\kappa)\mathbf{P}_z(\kappa)\Phi^T(\kappa) + \Gamma(\kappa)\mathbf{P}_\xi(\kappa)\Gamma^T(\kappa) . \quad (13)$$

### 3.3 Optimal dynamic RSS filtering technique

The strategy is to design an optimal decision procedure that, when applied to all RSS observations will provide an optimal solution to the state vector  $\mathbf{z}(\kappa)$  subjected to its prior defined dynamic model given by the stochastic dynamic equation (9). The estimate of the state vector optimally defined in the sense of the Bayesian minimum risk strategy (Shkvarko, 2004) in discrete time  $\kappa$  can be represented in the conditioned form

$$\hat{\mathbf{z}}_{opt}(\kappa) = \langle \mathbf{z}(\kappa) | \Sigma(0), \Sigma(1), \dots, \Sigma(\kappa) \rangle , \quad (14)$$

where  $\langle \cdot \rangle$  represents an ensemble averaging operator. For discrete time, the design procedure is based on the concept of mathematical induction (Falkovich et al., 1989). This is a supposition that after  $\kappa$  observations  $\{\Sigma(0), \Sigma(1), \dots, \Sigma(\kappa)\}$  the desired optimal estimate is produced, defined at the ultimate step as

$$\hat{\mathbf{z}}_{opt}(\kappa) = \hat{\mathbf{z}}_{opt}(\kappa) . \quad (15)$$

In order to use the estimate  $\hat{\mathbf{z}}_{opt}(\kappa)$  it is necessary to design an algorithm that produces the optimal estimate  $\mathbf{z}(\kappa+1)$  incorporating new measurements  $\Sigma(\kappa+1)$  according to the state dynamic equation (9). This is, we have to design an optimal decision procedure (optimal

filter) that, when applied to all reconstructed RSS maps  $\{\Sigma(\kappa)\}$  ordered in discrete time  $\kappa$  ( $\kappa_0 \rightarrow \kappa$ ), provides an optimal reconstruction of the desired RSS map represented via the estimate of the state vector  $\mathbf{z}(\kappa)$  subject to the numerical dynamic model (9). To proceed with derivation of such a filter, we first represent the state dynamic equation (9) in discrete time  $\kappa$  as follows

$$\mathbf{z}(\kappa+1) = \Phi(\kappa)\mathbf{z}(\kappa) + \Gamma(\kappa)\xi(\kappa) . \quad (16)$$

### 3.4 Dynamic RSS map reconstruction

According to the dynamical model of equation (16), the anticipated mean value for the state vector can be expressed as (Villalon & Shkvarko, 2008)

$$\mathbf{m}_z(\kappa+1) = \langle \mathbf{z}(\kappa+1) \rangle = \langle \mathbf{z}(\kappa+1) | \hat{\mathbf{z}}(\kappa) \rangle . \quad (17)$$

The  $\mathbf{m}_z(\kappa+1)$  is considered as the a priori conditional mean value of the state vector for the  $(\kappa+1)$ -st estimation step, thus, from equations (16) and (17) we obtain

$$\mathbf{m}_z(\kappa+1) = \Phi \langle \mathbf{z}(\kappa) | \Sigma(0), \Sigma(1), \dots, \Sigma(\kappa) \rangle + \Gamma \langle \xi(\kappa) \rangle = \Phi \hat{\mathbf{z}}(\kappa) , \quad (18)$$

hence, the prognosis of the mean value becomes

$$\mathbf{m}_z(\kappa+1) = \Phi \hat{\mathbf{z}}(\kappa) . \quad (19)$$

From the analysis of equations (16) thru (19), it is possible to deduce that given the fact that the particular RSS map  $\Sigma(\kappa)$  is treated at discrete time  $\kappa$ , it makes the previous reconstructions  $\{\Sigma(0), \Sigma(1), \dots, \Sigma(\kappa)\}$  irrelevant; hence, the optimal filtering strategy is reduced to the dynamical one step predictor described by the equation (16). Using these derivations, the dynamical estimation strategy can be modified to the one step optimal prediction procedure (Villalon & Shkvarko, 2008)

$$\begin{aligned} \hat{\mathbf{z}}(\kappa+1) &= \langle \mathbf{z}(\kappa+1) | \Sigma(0), \Sigma(1), \dots, \Sigma(\kappa), \Sigma(\kappa+1) \rangle = \langle \mathbf{z}(\kappa+1) | \hat{\mathbf{z}}(\kappa); \Sigma(\kappa+1) \rangle ; \\ \hat{\mathbf{z}}(\kappa+1) &= \langle \mathbf{z}(\kappa+1) | \Sigma(\kappa+1); \mathbf{m}_z(\kappa+1) \rangle . \end{aligned} \quad (20)$$

For the current  $(\kappa+1)$ -st discrete time estimation/prediction step, the dynamical RSS map estimate of the equation (8) in discrete time becomes

$$\Sigma(\kappa+1) = \mathbf{H}(\kappa+1)\mathbf{z}(\kappa+1) + \mathbf{v}(\kappa+1) , \quad (21)$$

with the a priori predicted mean calculated by the equation (17) for the desired state vector given by (16). Applying the Wiener minimum risk strategy (Shkvarko, 2004) to solve the equation (21) with respect to the state vector  $\mathbf{z}(\kappa)$  and taking into account the a priori infor-

mation summarized by the equations (10) thru (12), we obtain the dynamic solution for the RSS map state vector

$$\hat{\mathbf{z}}(\kappa+1) = \mathbf{m}_z(\kappa+1) + \mathbf{\Theta}(\kappa+1)[\mathbf{\Sigma}(\kappa+1) - \mathbf{H}(\kappa+1)\mathbf{m}_z(\kappa+1)] , \quad (22)$$

where the desired dynamic filter operator  $\mathbf{\Theta}(\kappa+1)$  is defined as (Villalon & Shkvarko, 2008)

$$\mathbf{\Theta}(\kappa+1) = \mathbf{K}_\theta(\kappa+1)\mathbf{H}^T(\kappa+1)\mathbf{P}_v^{-1}(\kappa+1) , \quad (23)$$

and

$$\mathbf{K}_\theta(\kappa+1) = [\mathbf{\Psi}_\theta(\kappa+1) + \mathbf{P}_z^{-1}(\kappa+1)]^{-1} , \quad (24)$$

$$\mathbf{\Psi}_\theta(\kappa+1) = \mathbf{H}^T(\kappa+1)\mathbf{P}_v^{-1}(\kappa+1)\mathbf{H}(\kappa+1) . \quad (25)$$

Finally, using the derived filter equations (22) thru (25) and the initial RSS map state model of equation (9), the optimal filtering procedure for the dynamic reconstruction of the desired RSS map can be represented in discrete time  $\kappa$  as

$$\hat{\mathbf{\Lambda}}(\kappa+1) = \mathbf{\Phi}(\kappa)\hat{\mathbf{z}}(\kappa) + \mathbf{\Theta}(\kappa+1)[\mathbf{\Sigma}(\kappa+1) - \mathbf{H}(\kappa+1)\mathbf{\Phi}(\kappa)\hat{\mathbf{z}}(\kappa)] ; \quad \kappa=0,1, \dots , \quad (26)$$

#### 4. Geophysical Dynamic Laboratory

The described technique provides the dynamical RSS map based on the atlas of RSS maps extracted from MRS scenes.

The GDL method is defined in the form of equation (26) based on the atlas of RSS maps in discrete time as follows

$$\hat{\mathbf{\Lambda}}_{GDL} = \hat{\mathbf{\Lambda}}(\kappa+1) = \mathbf{\Phi}(\kappa)\hat{\mathbf{z}}(\kappa) + \mathbf{\Theta}(\kappa+1)[\mathbf{\Sigma}(\kappa+1) - \mathbf{H}(\kappa+1)\mathbf{\Phi}(\kappa)\hat{\mathbf{z}}(\kappa)] . \quad (27)$$

Here, the observation vector  $\mathbf{\Sigma}$  is formed by the threshold values of the same  $(i, j)$ -th pixel through the different RSS maps of the atlas in the discrete time  $\kappa$ .

The estimate vector  $\mathbf{z}$  is formed by the estimation values  $\mathbf{\Lambda}$  one step prior in the same current discrete time. Fig. 5 shows the detailed computational structure of the GDL method for the environmental RSS extraction from MRS imagery.

#### 5. Simulation Experiments for Hydrological Signatures

In the reported here simulation results, hydrological RSS electronic maps are extracted from high-resolution MRS images. Three level RSS are selected for this particular simulation processes, moreover, unclassified zones are also considered (2-bit classification) and are described as follows.

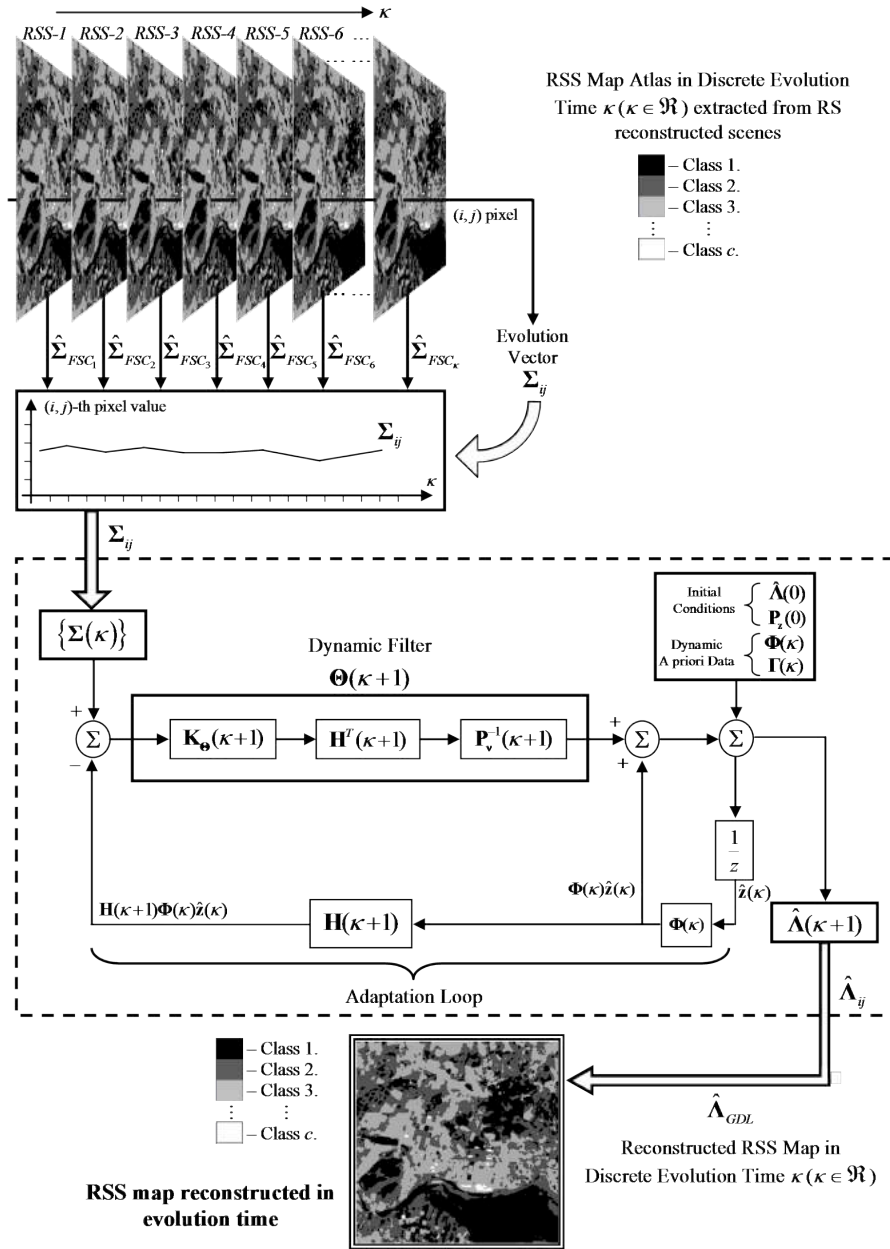






Fig. 5. Computational structure of the GDL method

-  - Black regions represents the RSS relative to the wet zones of the MRS image.
-  - Heavy-gray regions represents the RSS relative to the humid zones of the MRS.
-  - Light-gray regions represents the RSS relative to the dry zones of the MRS.
-  - White regions represent the unclassified zones of the RSS map.

### 5.1 Multispectral Image Classification

To analyze the overall performance of the WPS technique, a set of four high-resolution (1024x1024-pixels) MRS scenes in TIFF format are used, borrowed from diverse zones in Mexico.

A comparison with the results obtained with the classical WOS and MDM methods is provided. Figs. 6(a), 7(a), 8(a) and 9(a) show the four different MRS scenes, respectively.

To perform the qualitative study, Figs. 6(b), 7(b), 8(b) and 9(b) show the results obtained with the WOS method for each scene, respectively.

Figs. 6(c), 7(c), 8(c) and 9(c) show the results obtained with the MDM method for each scene, respectively.

Figs. 6(d), 7(d), 8(d) and 9(d) show the results obtained with the WPS method for each scene, respectively.

The quantitative study is performed calculating the classified percentage obtained with the WOS, MDM and WPS methods, respectively, and compared with the original class quantities from the original MRS scenes. Tables 1, 2, 3 and 4 show the quantitative results.

The theory of the WOS method defines that the classification is performed only using one band (Jensen, 2005), for this simulation the G band was used. The resulting RSS map shows a large unclassified zone, this is due to the color gradient present on the original MRS image and the lack of supervised data.

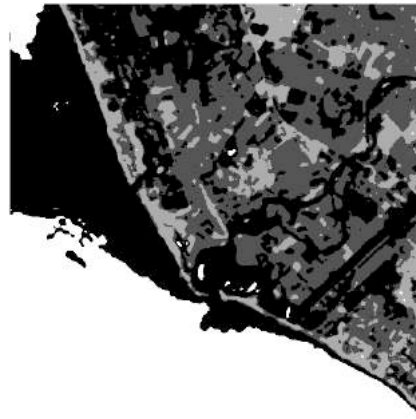
The MDM method uses the three RGB bands (Jensen, 2005). The WPS method also uses the three RGB bands to analyze the pixel-level means and variances to perform a more accurate segmentation and classification; therefore, using the statistical pixel-based information the RSS map obtained shows a high-accurate classification without unclassified zones. From the details shown in Figures 6 thru 9, the WPS method performs a more accurate and less smoothed identification of the classes.

Tables 1 to 4 show the quantitative performances. From this analysis, the WPS classified image provides a lower percentage difference from the original MRS scenes than the WOS or MDM classified images. Moreover, the WOS and MDM reveal some unclassified zones due to their respective decision rules (Johannsen et. al, 2003); the WPS method classifies all the pixels due to the use of pixel-based statistical training data.

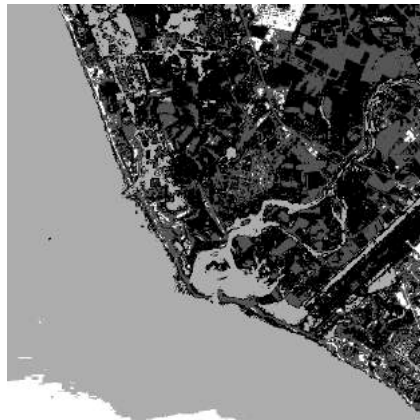
These qualitative and quantitative results probe the overall performance of the developed WPS technique.



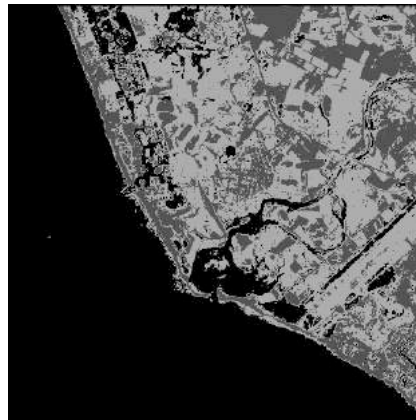
a. Original high-resolution MRS scene



b. RSS map extracted with the WOS method



c. RSS map extracted with MDM method



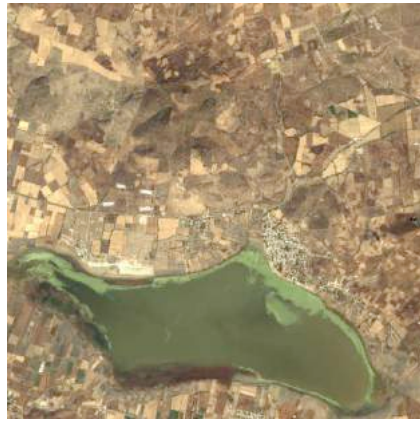
d. RSS map extracted with the WPS method

Fig. 6. Simulation results for hydrological RSS map extraction from the first MRS scene

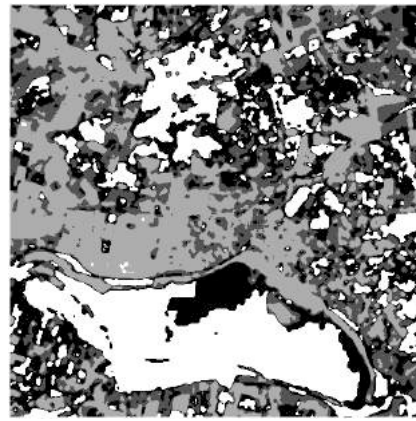
Method →	Original	WOS method		MDM method		WPS method	
	Base [%]	%	Diff.	%	Diff.	%	Diff.
Wet	34.34	35.37	-1.03	31.93	+2.41	50.09	-15.74
Humid	32.60	26.75	+5.85	17.00	+15.61	18.37	+14.3
Dry	33.06	9.45	+23.61	47.18	-14.12	31.54	+1.51
Unclass.	-----	28.43	+28.43	3.90	+3.90	0.00	+0.00
<b>Percentage Points Difference →</b>			58.92%	36.04%	<b>31.5%</b>		

Table 1. Comparative table of the hydrological RSS percentages obtained with the classification methods from the first MRS scene





a. Original high-resolution MRS scene



b. RSS map extracted with the WOS method



c. RSS map extracted with MDM method



d. RSS map extracted with the WPS method

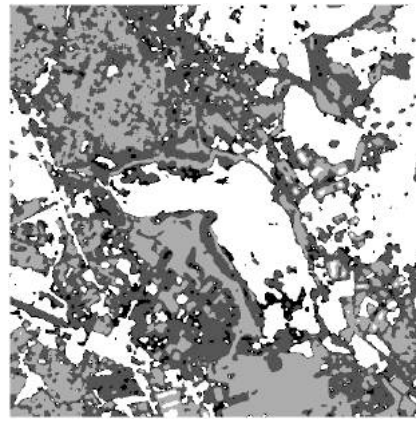
Fig. 7. Simulation results for hydrological RSS map extraction from the second MRS scene.

Method →	Original	WOS method		MDM method		WPS method	
	Base [%]	%	Diff.	%	Diff.	%	Diff.
Wet	33.11	23.66	+9.45	29.53	+5.57	51.22	-18.12
Humid	33.11	21.78	+11.32	21.24	+13.87	19.79	+13.3
Dry	33.79	27.03	+6.76	50.06	-16.28	28.99	+4.83
Unclass.	-----	27.53	+27.53	1.17	+1.17	0.00	+0.00
<b>Percentage Points Difference →</b>			55.05%	36.88%	<b>36.2%</b>		

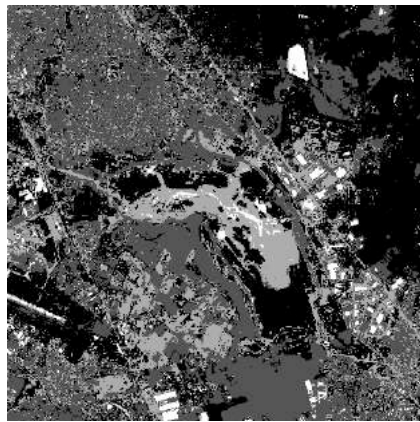
Table 2. Comparative table of the hydrological RSS percentages obtained with the classification methods from the second MRS scene.



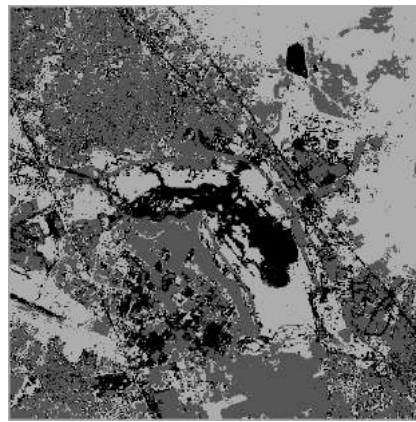
a. Original high-resolution MRS scene



b. RSS map extracted with the WOS method



c. RSS map extracted with MDM method



d. RSS map extracted with the WPS method

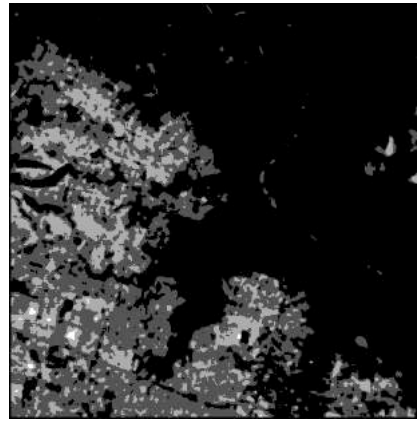
Fig. 8. Simulation results for hydrological RSS map extraction from the third MRS scene.

Method →	Original	WOS method		MDM method		WPS method	
	Base [%]	%	Diff.	%	Diff.	%	Diff.
Wet	33.02	6.87	+26.15	40.98	-7.96	21.31	+11.7
Humid	33.09	33.30	-0.22	35.38	-2.29	36.38	-3.31
Dry	33.89	23.07	+10.82	20.66	+13.23	42.31	-8.43
Unclass.	-----	36.75	+36.75	2.98	+2.98	0.00	+0.00
<b>Percentage Points Difference →</b>			73.94%		26.45%		<b>23.4%</b>

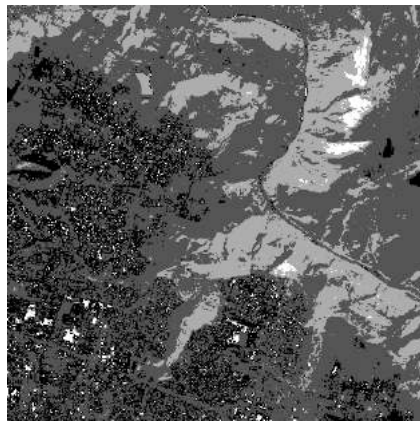
Table 3. Comparative table of the hydrological RSS percentages obtained with the classification methods from the third MRS scene.



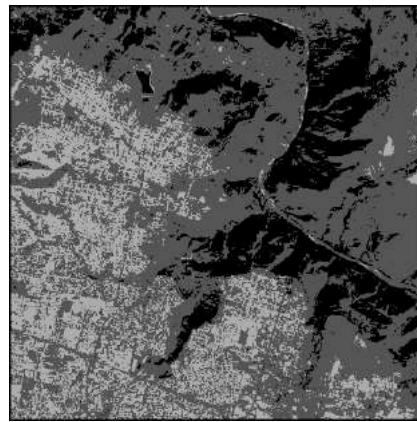
a. Original high-resolution MRS scene



b. RSS map extracted with the WOS method



c. RSS map extracted with MDM method



d. RSS map extracted with the WPS method

Fig. 9. Simulation results for hydrological RSS map extraction from the fourth MRS scene.

Method →	Original	WOS method		MDM method		WPS method	
	Base [%]	%	Diff.	%	Diff.	%	Diff.
Wet	32.41	65.35	-32.94	19.06	+13.35	20.62	+11.8
Humid	34.13	25.52	+8.61	60.14	-26.00	58.95	-24.82
Dry	33.46	9.03	+24.42	18.22	+15.23	20.43	+13.1
Unclass.	-----	0.10	+0.10	2.58	+2.58	0.00	+0.00
<b>Percentage Points Difference →</b>			66.07%		57.16%		<b>49.6%</b>

Table 4. Comparative table of the hydrological RSS percentages obtained with the classification methods from the fourth MRS scene.

## 5.2 Dynamical Analysis

A set of hydrological RSS electronic maps were extracted from 40 MRS high-resolution images of a particular scene obtained with the same time interval (discrete time).

The GDL dynamic post-processing method is applied to the high-resolution collection of RSS map (Shkvarko & Villalon, 2007) based on the computational structure described in Fig. 5. First, the collection of 40 RSS maps (Marple, 1987) collected in different time of the same scene is set for the simulation. Therefore, the discrete time  $\kappa = 40$ . Second, the pixel evolution vector  $\Sigma_{ij}$  is defined for this simulation as

$$\Sigma_{ij} = \left( \hat{\Sigma}_{ij,1} \quad \hat{\Sigma}_{ij,2} \quad \hat{\Sigma}_{ij,32} \right), \quad (28)$$

where  $\hat{\Sigma}$  represents the threshold values of the same  $(i, j)$ -th pixel from the 40 RSS maps. This is the observation signal to be post-processed with the dynamic post-processing method.

Third, the measurement matrix  $\mathbf{H}$  and the state transition matrix  $\Phi$  are simplified to  $\mathbf{I}$  because the equation of observation (9) and the stochastic dynamic state equation (21) are supposed to be ideal (noiseless, because the observation vector is directly extracted from the RSS maps). The dynamic filter operator (gain matrix)  $\Theta$  determines the variance evolution of the observation values (28) of the dynamically reconstructed RSS. The initial conditions are the initial observation value  $\Sigma(0)$  and its initial estimation  $\hat{\Lambda}(0) = \Lambda\{\Sigma(0)\}$ .

The GDL method specified by equation (25) is applied to estimate the ultimate value  $\hat{\Lambda}$  that is the next  $(\kappa + 1)$ -st evolution time step of the observation vector  $\Sigma_{ij}$ . This represents the dynamic filtration of the desired RSS from the reconstructed observation data and can be expressed as

$$\hat{\Lambda}_{ij} = \hat{\Lambda}(\kappa + 1). \quad (29)$$

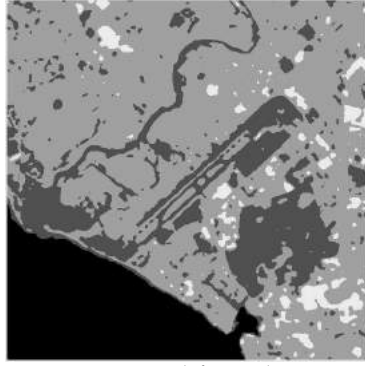
This process is performed through all the  $\{(i, j)\}$  pixels of the 40 RSS maps to obtain a single aggregated RSS map  $\hat{\Lambda}_{GDL}$ . The simulation results of application of the developed GDL method are presented in Figs. 10 and 11.

Figs. 10(a) thru 10(e) show the first five high-resolution ( $1024 \times 1024$ -pixel) hydrologic RSS maps extracted from the first five MRS scenes (corresponding to the Banderas Bay of Puerto Vallarta in Mexico) in different evolution time ( $\kappa=1, 2, 3, 4$  and  $5$ ), respectively.

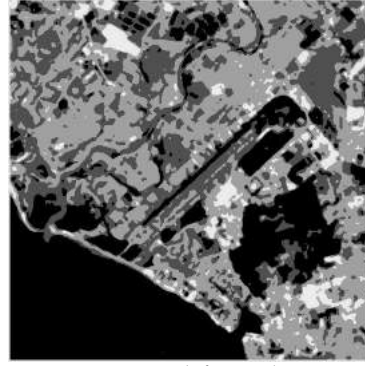
Fig. 10(f) shows the dynamic RSS map reconstructed with the application of the GDL method for the  $\kappa+1$  time step ( $\kappa=41$ ) specified by the computational structure described in Fig. 5.

Fig. 11(a) shows the first original high-resolution ( $1024 \times 1024$ -pixel) MRS scene ( $\kappa=1$ ). Fig. 11(b) shows the dynamic MRS map reconstructed with the application of the GDL method for the  $\kappa=41$  time step.

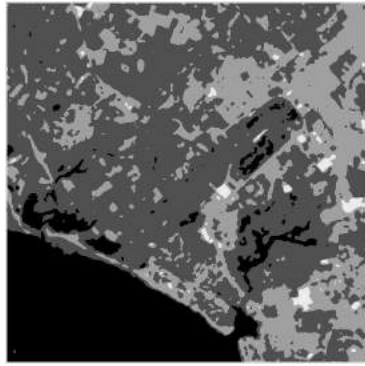
The RSS maps were reconstructed in discrete time  $\kappa$ , therefore, the GDL method produces the desired dynamic RSS prediction of the RSS map for the next time step  $(\kappa + 1)$ ; where  $\kappa = 0, 1, \dots$



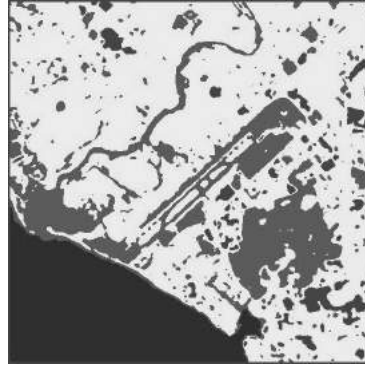
a. RSS map extracted from the MRS scene for a  $\kappa = 1$  discrete time step



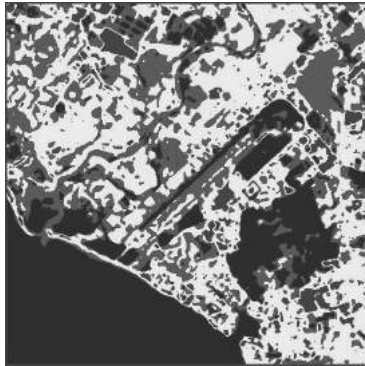
b. RSS map extracted from the MRS scene for a  $\kappa = 2$  discrete time step



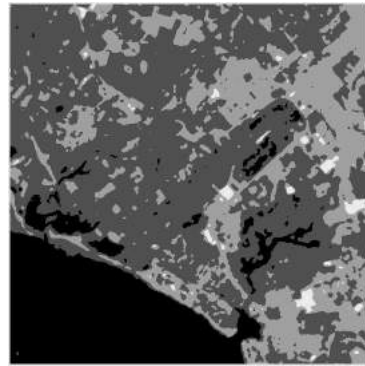
c. RSS map extracted from the MRS scene for a  $\kappa = 3$  discrete time step



d. RSS map extracted from the MRS scene for a  $\kappa = 4$  discrete time step



e. RSS map extracted from the MRS scene for a  $\kappa = 5$  discrete time step



f. RSS dynamic prediction obtained with GDL for the  $\kappa = 41$  discrete time step

Fig. 10. Simulation results for dynamic RSS map analysis.



a. Original high-resolution MRS scene for the  $\kappa = 1$  discrete time step      b. High-resolution MRS scene predicted for the  $\kappa = 41$  discrete time step

Fig. 11. Simulation results for dynamic MRS map analysis.

## 6. Summary of Computational Algorithms

The detailed stages of the computational algorithm for the WPS and GDL methodologies are summarized as follows.

### 6.1 Weighted Pixel Statistics method

1. Set the number of RSS to classify.
2. Select one point on the MRS image for each class to be classified.
3. Separate the spectral RGB band from the true-color MRS image.
4. The selected points determine the training weights that consist of the means matrix  $\mathbf{M}$  and the variances matrix  $\mathbf{V}$ . These matrixes contain the mean and variance of each point in the R, G and B bands, respectively.
5. For each  $(i, j)$ -th pixel in the R, G and B bands, respectively, perform the following process
  - Set a  $5 \times 5$  pixel neighbourhood shift window  $\mathbf{W}$ .
  - Determine the mean of the shift window  $\mathbf{W}$ .
  - Determine the variance of the shift window  $\mathbf{W}$ .
  - Calculate the Euclidean distances between the means and the training means for each band and for each class (Fig. 3).
  - Calculate the Euclidean distances between the variance and the training variances for each band and for each class (Fig. 3).
  - Select the minimum class distance for the means.
  - Select the minimum class distance for the variances.
  - Perform a comparison between the class distance for the mean and the class distance for the variance, and classify the pixel according to the minimum value and the class from which is obtained.

## 6.2 Geophysical Dynamic Laboratory method

1. Set a collection of discrete time ( $\kappa$ ) RSS maps from the electronic atlas extracted from the MRS imagery for a particular scene.
2. For each  $(i, j)$ -th pixel on the RSS maps perform the following process:
  - Set the pixel-based evolution vector  $\Sigma_{ij}$ , which contains the threshold RSS values for the pixel in discrete evolution time  $\kappa$ .
  - Apply the GDL method to the vector  $\Sigma_{ij}$  (Fig. 5) to obtain the dynamic prediction  $\hat{\Lambda}(\kappa+1)$ , which conform the matrix  $\hat{\Lambda}_{ij}$ .
3. The reconstructed  $\hat{\Lambda}_{ij}$  matrix conform the  $\hat{\Lambda}_{GDL}$  dynamic RSS image in discrete time  $\kappa$ .

## 7. Conclusion

The extraction of remote sensing signatures from a particular geographical region allows the generation of electronic signature maps, which are the basis to create a high-resolution signatures atlas processed in discrete time, and moreover, perform its dynamical analysis. This chapter analyzed the implementation possibilities of the WPS and GDL methods for hydrological resources management based geophysical applications. The extraction of hydrological RSS from high-resolution MRS imagery was reported to probe the efficiency of the developed techniques.

### 7.1 Multispectral Image Classification

From the simulation results one may deduce that the WOS classifier generates several unclassified zones; while the MDM classifier is more accurate because it uses more robust information in the processing (several image spectral bands), nevertheless, despite the fact that few zones are unclassified, the results have considerable density of unity pixels (sufficient for decision making based on these extracted RSS). The developed WPS method provides the high resolution environmental RSS electronic map with a high-accurate classification and without unclassified zones. This is achieved because the WPS method uses the three RGB bands to analyze the pixel-level means and variances to perform a more accurate segmentation and classification; therefore, using the statistical pixel-based information the RSS map obtained shows a high-accurate classification without unclassified zones. The resulting RSS map ensures better results in the classification achieved with the developed WPS method. This is probed by the RSS percentages obtained with the WPS method, which manifest the lowest percentage difference to those obtained with the WOS and MDM classification techniques. Also, the WPS method for RSS extraction can be applied to several MRS images of a particular geographical region obtained in different moments of time (discrete time), to generate a RSS atlas of environmental electronic maps. This process is a powerful tool for geophysical resource management.

### 7.2 Dynamical Analysis

The GDL method provides a possibility to perform the high-resolution intelligent analysis of the dynamic behavior or the desired environmental RSS map model with a high-accurate classification of the particular RSS map evolution.

This is achieved because the GDL algorithm aggregates the RSS map atlas information for a particular MRS scene in discrete evolution time and employs more detailed robust a priori

information from the original MRS scene. The resulting dynamic RSS prediction map ensures high-accurate estimation results in the classification achieved with the developed GDL method. The reported here simulation results shows the qualitative and quantitative analysis of the overall performance of the WPS and GDL methods for remote sensing signatures analysis. The application as an auxiliary tool in Geophysical information retrieval and data interpretation for land use management and analysis are a matter of further studies.

## 8. References

- Falkovich S.; Ponomaryov V. & Shkvarko Y. (1989). *Optimal Spatial-Temporal Signal Processing for Spread Radio Channels*, Radio and Communication Press, U.S.S.R.
- Fussell J.; Rundquist D. & Harrington J. (1986). On defining remote sensing. *Journal of Photogrammetric Engineering & Remote Sensing*, Vol. 52, 1507-1511
- Grewal M. & Andrews A. (2001). *Kalman Filtering: Theory and Practice using Matlab*, John Wiley & Sons, U.S.A.
- Jensen J. (2005). *Introductory Digital Image Processing: A Remote Sensing Perspective*, Prentice-Hall, U.S.A.
- Johannsen C.; Petersen G.; Carter P. & Morgan M. (2003). Remote sensing: changing natural resource management. *Journal of Soil & Water Conservation*, Vol. 58, 42-45
- Luenberger D. (1979). *Introduction to Dynamic Systems: Theory, Models and Applications*, John Wiley & Sons, U.S.A.
- Marple S. (1987). *Digital Spectral Analysis*, Prentice-Hall, U.S.A.
- Mather P. (2004). *Computer Processing of Remotely-Sensed Images*, John Wiley & Sons, U.S.A.
- Perry S.; Wong H. & Guan L. (2002). *Adaptive Image Processing: A Computational Intelligence Perspective*, CRC Press, U.S.A.
- Shkvarko Y. (2004). Unifying regularization and bayesian estimation methods for enhanced imaging with remotely sensed data. Part I - theory. *IEEE Transactions on Geoscience and Remote Sensing*, Vol. 42, 923-931
- Shkvarko Y. & Villalon I. (2007). Remote sensing imagery and signature field reconstruction via aggregation of robust regularization with neural computing, In: *Lecture Notes in Computer Sciences*, Blanc-Talon J.; Philips W.; Popescu D. & Scheunders P. (Ed.), pp. 235-246, Springer Verlag, Germany
- Smith S. (2000). *The Scientist and Engineer's Guide to Digital Signal Processing*, Web Edition, U.S.A.
- Villalon I. & Shkvarko Y. (2008). Comparative study of the descriptive experiment design and robust fused bayesian regularization techniques for high-resolution radar imaging. *Scientific and Technical Journal on Radioelectronics and Informatics*, Vol. 1, 34-48
- Villalon I. (2008). Weighted pixel statistics for multispectral image classification of remote sensing signatures: performance study, *Proceedings of the 5<sup>th</sup> IEEE International Conference on Electrical Engineering, Computing Science and Automatic Control*, pp. 534-539, IEEE Press, Mexico City
- Yli-Harja O.; Astola J. & Neuvo Y. (1991). Analysis of the properties of median and weighted order median filters using threshold logic and stack filter representations. *IEEE Transactions on Signal Processing*, Vol. 39, 395-410